

# Fabrication and experimental characterization of a sol–gel derived nanostructured n-ZnO/p-Si heterojunction diode

Satyendra Kumar Singh<sup>1</sup> · Purnima Hazra<sup>2</sup> · Shweta Tripathi<sup>1</sup> · P. Chakrabarti<sup>1,3</sup>

Received: 26 April 2015 / Accepted: 29 June 2015 / Published online: 7 July 2015  
© Springer Science+Business Media New York 2015

**Abstract** In this paper, fabrication and characterization of a sol–gel derived n-ZnO nanoparticle/p-Si heterojunction diode has been presented. A strong diffraction peak (002) obtained from XRD spectra of sol–gel derived ZnO thin film indicates that the growth of hexagonal wurtzite ZnO nanoparticles are preferably along the c-axis. The surface morphological features extracted from AFM and SEM images predict the uniform growth of ZnO nanoparticles over the p-Si substrate. The optical properties of ZnO nanoparticles have been measured in the spectral range of 300–1000 nm using ellipsometer and photoluminescence spectroscopy. The optical transmittance of ZnO nanoparticles has been observed between 81 and 92.66 % in visible region and the optical band gap has been found out to be 3.24 eV. Finally, metallic contacts were deposited on top of ZnO layer and bottom of Si layer to perform electrical characterization of nanostructured n-ZnO/p-Si heterojunction diodes. Electrical parameters including reverse saturation current, ideality factor, barrier height, rectification ratio have been calculated to explore the potential of the device for futuristic nanoelectronic and optoelectronic device applications.

## 1 Introduction

Zinc oxide (ZnO) is an inherently n-type transparent semiconductor with large exciton binding energy of 60 meV and wide band gap of 3.37 eV at room temperature [1, 2]. It is a low cost, nontoxic material, having high electrochemical stability [3, 4]. Nanostructured ZnO-based devices have drawn significant attention of the researchers over the past decade for their possible deployment in a variety of electronic and optoelectronic applications. ZnO can easily form a wide range of nanostructures with unique electrical and optical properties, depending on the experimental conditions, such as type of substrate, deposition method, type of seed layer, deposition temperature and deposition conditions [1, 4–6]. These nanostructure-based devices have found wide spread applications in solar cells, gas sensors, memory devices, and ultraviolet photodetectors [7–12]. ZnO-based ultraviolet photodetectors have potential advantages that include its strong UV-response, feasibility of simple and low cost processing, and chemical stability even in adverse environment [9–11]. Researchers have reportedly used a variety of techniques for growing ZnO nanostructures for fabrication of Schottky contact, MSM, MISIM, heterojunction diodes. The deposition techniques include RF/DC magnetron sputtering, vacuum thermal evaporation deposition techniques [1, 2, 5, 13, 14]. Among these techniques, the sol–gel process is by the most convenient one for possible integration of ZnO-based devices onto Silicon wafers containing CMOS integrated circuits. This is because the sol gel technique offers the possibility of excellent compositional control, simplicity of deposition irrespective of the nature of substrate, homogeneity in the derived film, lower crystallization temperature and low production costs [11, 14, 15]. Various research groups, viz. Gadallah et al. [3], Sahal et al. [4], Yakuphanoglu et al. [11], Huang et al. [14] have

✉ P. Chakrabarti  
pchakrabarti.ece@itbhu.ac.in

<sup>1</sup> Motilal Nehru National Institute of Technology,  
Allahabad 211004, India

<sup>2</sup> Shri Mata Vaishno Devi University, Kakaryal, Katra 182320,  
India

<sup>3</sup> Indian Institute of Technology, Banaras Hindu University,  
Varanasi 221005, India

reported synthesis of ZnO thin film using sol–gel route followed by either spin coating or deep coating technique. The as-deposited sol–gel-spin-coat derived ZnO nanostructures have been extensively used for making electronic and optoelectronic devices. Chen et al. [10] have reported contrast ratio as nearly 100 at 5 V bias voltage for their ZnO nano-pillar based Schottky contact photodetector fabricated by sol–gel spin coating technique. Yakuphanoglu et al. [11] have fabricated and characterized ZnO nanostructure/Si heterojunction for photodetection and photovoltaic applications. Foo et al. [12] have demonstrated Si/SiO<sub>2</sub>/ZnO nanoparticles based MSM UV photodetector structure using sol–gel spin coating technique and evaluated contrast ratio (photo to dark current ratio) as only 4.82 under 1.16 mW UV light at 5 V bias voltage. Ali and Chakrabarti [13] have fabricated and characterized a ZnO thin film based Schottky contact photodetector using sol gel spin coating technique. The device is reported to exhibit a responsivity of 0.2137 A/W and a contrast ratio as 8 at 3 V reverse bias voltage. It can be observed from the above survey that although sol–gel technique is a low cost and easy to handle technique but researchers have not yet fully explored the potential of this technique for developing useful ZnO nanostructure based electronic devices. The present work makes a systematic study of the detailed structural, surface morphological analysis involving roughness, grain size, lattice parameters, defect density, stress, strain measurements and optical analysis of sol–gel derived ZnO nanostructures in respect of transmittance, reflectance, optical bandgap, refractive index, dielectric constant, surface and volume energy loss function, photoluminescence measurements. The transparent and semiconducting ZnO nanoparticles prepared by sol–gel technique were directly grown on pre-cleaned p-type silicon substrate using spin coating method. A complete characterization of the n-ZnO nanoparticle/p-Si heterojunction photodetector fabricated using the sol–gel spin coating technique was subsequently carried out. The electrical parameters such as ideality factor, reverse saturation current, barrier height and UV photodetection properties including photo-responsivity and contrast ratio of proposed ZnO nanoparticles/Si heterojunction diode have also been measured and reported in this article.

## 2 Experimental procedure

In the present study, ZnO was deposited on p-Si (100) substrate (thickness  $\sim 380 \mu\text{m}$  and resistivity  $\sim 3\text{--}7 \Omega\text{-cm}$ ) by sol–gel spin coating technique. Zinc acetate dehydrate ( $\text{ZnCH}_3(\text{COO})_2 \cdot 2\text{H}_2\text{O}$ ) has been used as a starting material to prepare zinc oxide sols for spin coating technique. Zinc acetate dehydrate is a cheap material and has a good solubility in alcohols as compared with

alkoxides, such as zinc-n-propoxide [13]. In order to obtain the sols, the precursor zinc acetate dehydrate was first dissolved into isopropanol ( $(\text{CH}_3)_2\text{CHOH}$ ) which acts as a solvent and then diethanolamine was added in the solution as a stabilizer. Molar ratio of diethanolamine to zinc acetate was maintained at 1:1 and the concentration of zinc acetate dehydrate was 0.2 M. 4.3902 g of zinc acetate dehydrate was dissolved in 40 ml of isopropanol and stirring at 343 K up to 30 min. When the whitish frozen structure was obtained in the process, 2.102 g of diethanolamine was added followed by continuous stirring. The milky ice was broken and after around 20 min, a transparent sol was obtained. The transparent sol was subjected to continuous stirring for 3–4 h at 313 K so as to obtain clear and homogeneous solution. The sol was placed at room temperature to be aged for 24 h. Prior to deposition by spin coating technique, the p-type Si substrate (wafer of 4" diameter) was cut into small stripes of size  $0.75' \times 0.75'$  and degreased through RCA-1 and RCA-2 (Radio Corporation of America) process to remove the organic and ionic contaminants respectively [16]. After completion of RCA cleaning, Si substrate was rinsed thoroughly by deionized (DI) water for 6–8 times. The dried substrate was mounted on the sample holder of the spin coater. The sol was poured on substrate and sample holder was rotated at a speed of 2000 and 3000 rpm for 10 and 20 s respectively. After each cycle of spin coating, the substrate was post-dried on hot plate at 373 K for 15 min to evaporate the solvents and obtain the stable film. After each step, thickness of the film was measured by ellipsometer. This process was repeated for eight times to obtain the average thickness of 300 nm of as-grown ZnO layer. Thermal treatment was carried out at 673 K for 1 h to decompose the organic component from the film. Then, the ZnO film was annealed at 823 K for 1 h in open environment. The as-grown ZnO films were characterized using field emission scanning electron microscope (FESEM), atomic force microscopy (AFM), energy dispersive x-ray (EDX), X-ray diffraction (XRD), photoluminescence (PL) spectroscopy and ellipsometer to analyze the structural and optical parameters of the thin film.

Finally, ohmic contact was obtained on ZnO by depositing aluminium/titanium on the ZnO surface of the sample using RF magnetron sputtering at 13.56 MHz and  $0.5 \times 10^{-6}$  mbar pressure (HINDVAC, India system) with the help of shadow-masking technique. In the present case, a thin layer ( $\sim 20$  nm) of titanium is used below the aluminium contact as a buffer layer to prevent the diffusion of aluminium into the ZnO layer. The circular dots of 100 nm thickness were deposited using shadow mask containing an array of circular holes of diameter 1 mm each. For back ohmic contact, 150 nm thick aluminium layer was deposited by RF sputtering on the whole back surface of the Si

wafer. The device was subjected to post metallization annealing at 723 K for 20 min for passivation of top surface. The electrical properties of the diode were characterized by using semiconductor parameter analyzer. For characterization in respect of UV photodetection parameters, the heterojunction was exposed to UV light, at 365 nm wavelength with a power of 100 μW.

### 3 Results and discussion

#### 3.1 Structural properties

Figure 1 shows X-ray diffraction (XRD) spectra of the ZnO nanoparticle thin film. The strong diffraction peak corresponding to (200) orientation at  $2\theta = 34^\circ.48$  revealed the existence of a ZnO phase with a hexagonal wurtzite structure. Small peaks of XRD spectra corresponding to the planes (100), (101), (102), (110), (103) and (112) confirms the polycrystalline nature of as-grown ZnO nanoparticle thin film (JCPDS card no: 00-005-0664). Various important structural parameters including the average crystallite size, defect density, lattice constant, lattice strain and stress were extracted from the XRD measurements to analyze the nature of crystal growth of ZnO in details. The average crystallite size ( $D$ ) for (002) crystallographic plane [preferred orientation in XRD spectra] has been calculated as 19.9632 nm using Scherrer equation [3].

$$D = \frac{0.94\lambda}{\beta \cos \theta} \tag{1}$$

where  $\lambda = 1.54 \text{ \AA}$  is the wavelength of incident X-ray,  $\beta$  is full width at half maximum and  $\theta$  is the diffraction angle. Defect density ( $\delta$ ) is defined as the length of the dislocation line per unit volume and it is given as [3]:

$$\delta = \frac{1}{D^2} \tag{2}$$

The defect density ( $\delta$ ) is calculated using Eq. 2 to be  $2.509 \times 10^{-3} \text{ nm}^{-2}$ . It is a useful parameter to determine crystalline quality of as-grown thin film. The lower value of defect density provides the better quality of the crystalline nanostructures.

The lattice strain present in the nanoparticles can be determined using Eq. (3) [1]

$$\text{Lattice strain} = \frac{\beta}{4 \tan \theta} \tag{3}$$

The lattice parameters  $a$ ,  $b$  and  $c$  of the hexagonal structure are determined by Eqs. (4) and (5) [1]:

$$a = b = \frac{\lambda}{\sqrt{3} \tan \theta} \tag{4}$$

$$c = \frac{\lambda}{\sin \theta} \tag{5}$$

For hexagonal structure the lattice parameters  $a$  and  $b$  are same but the value of  $c$  is different from  $a$  and  $b$ . The calculated values for  $a = b$  and  $c$  are  $3.0086 \text{ \AA}$  and  $5.211 \text{ \AA}$  respectively. These values closely match with standard JCPDS data ( $a = b = 3.249 \text{ \AA}$  and  $c = 5.205 \text{ \AA}$ ) given for lattice parameters [1]. The residual stress ( $\sigma$ ) can be determined by Eq. (6) [1]:

$$\sigma = -233 \frac{(c - c_0)}{c_0} [\text{GPa}] \tag{6}$$

where,  $c_0$  is a constant which represents unstrained lattice. For bulk ZnO its value is  $5.2066 \text{ \AA}$ . The value obtained for residual stress is  $-0.2237 \text{ GPa}$ . The negative sign indicates the compressive nature of the stress.

#### 3.2 Study of surface morphology

The AFM images (2-D and 3-D) of a typical post-annealed sol-gel derived ZnO samples are shown in Fig. 2a, b. It is clearly seen from the images that ZnO nanoparticle thin film with uniform surface morphology can be grown on p-Si substrate using sol-gel spin coating technique. Roughness profile of the as-grown ZnO nanoparticle thin film for a scanning area of  $0.5 \mu\text{m} \times 0.5 \mu\text{m}$  is shown in Fig. 2c. The root mean square value of roughness was obtained as  $0.811 \text{ nm}$  for vertical scanning as shown in the figure. Here the profile height (nm) was taken along vertical axis and lateral position ( $\mu\text{m}$ ) was taken along horizontal axis. The nanoparticulate structure of ZnO thin film ensures that it has a special significance in the context of ultra violet detection. Scanning electron microscope (SEM) image of ZnO thin film at 250 K magnification is shown in Fig. 3a. From SEM image it has been observed that surface morphology of as-grown ZnO nanoparticle thin film is

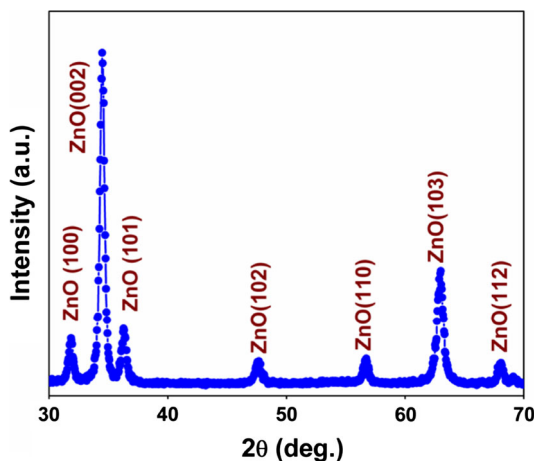
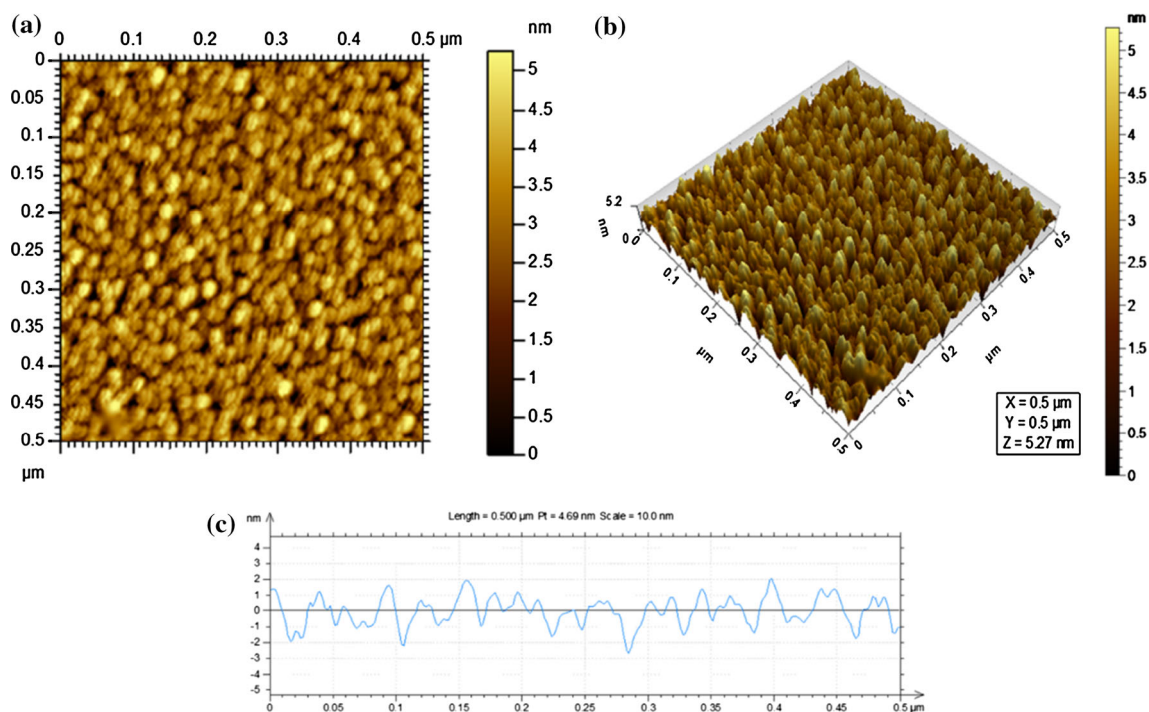
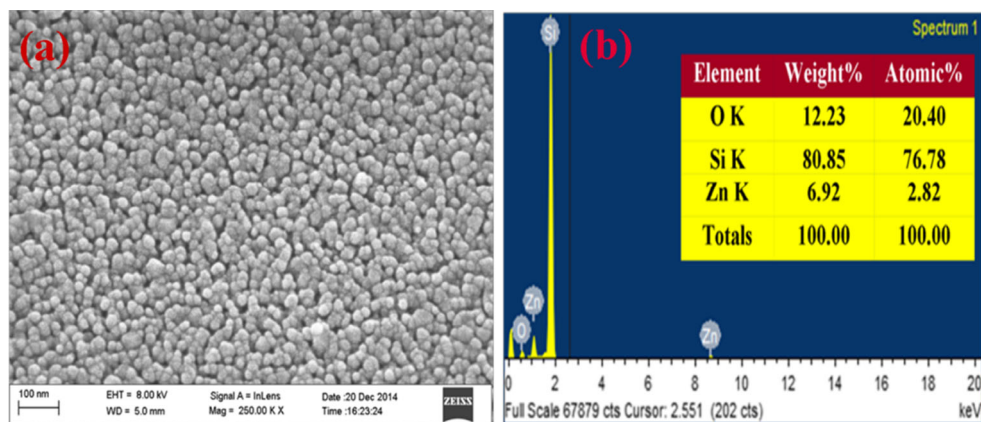


Fig. 1 XRD pattern for ZnO nanoparticle thin film



**Fig. 2** **a** 2-D and **b** 3-D AFM image of ZnO nanoparticle thin film on Si substrate, **c** Roughness plot of ZnO film

**Fig. 3** **a** SEM image and **b** EDX spectra of ZnO nanoparticle thin film (*inset*) table indicates the compositional analysis of as-grown sample



packed in a homogeneous and continuous fashion without the presence of any major porosity or voids.

Further, it can be noticed from SEM image that the film is having variable grain size in the range of 18–34 nm with almost round gain structures. Energy dispersive X-ray (EDX) spectra of ZnO nanoparticle thin film is shown in Fig. 3b. Zn and O peaks are clearly seen in the figure. Si peak seen in the spectra arises due to Si substrate. The weight% and atomic% of Zn, O and Si (due to Si substrate) are shown in Table 1 (obtained from EDX). Further, the results obtained from the table shown as an inset in Fig. 3b and EDX spectra assure that no other impurity is present in as-grown ZnO film.

### 3.3 Evaluation of optical properties

Figure 4 represents the transmittance and reflectance spectra from 300 to 800 nm of the nanoparticle thin film. The film was found to be transparent (81–92.66 %) in the visible range with a sharp absorption edge at a wavelength of about 390 nm, which is very close to that corresponding to the intrinsic bandgap of ZnO (3.24 eV). Low reflectance of ZnO thin film in visible region makes it a suitable choice for anti-reflecting coating materials in optoelectronic devices operated in this region. The reflection spectra vary from 10.8 to 17.3 % for 300–800 nm wavelength as shown in Fig. 4 (inset).

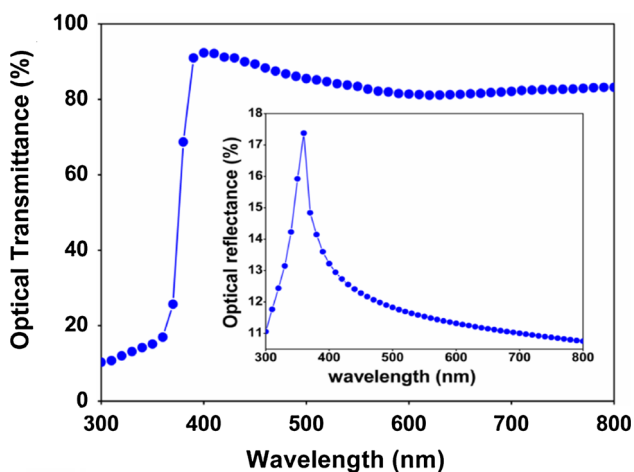


**Fig. 4** Transmittance spectra (*inset*) Reflectance spectra of as-grown ZnO thin film

The variation of the absorption coefficient ( $\alpha$ ) with the wavelength of light is shown in Fig. 5. The absorption coefficient is related to the transmittance and the film thickness is given by Beer–Lambert’s law [1]:

$$\alpha = \frac{2.303}{d} A = \frac{1}{d} \ln\left(\frac{1}{T}\right) \tag{7}$$

where, A is absorbance, T is the transmittance and d is thickness of ZnO thin film. The thickness (d) of thin film was measured by ellipsometer to be of the order of 300 nm. The variation of absorbance (A) of thin film as calculated on the basis of Eq. (7) is shown in Fig. 5 as an inset. It can be noted that for longer wavelengths ( $\lambda > 380$  nm), the weaker absorbance (<20 %) and for shorter wavelengths ( $\lambda < 380$  nm) the stronger absorbance (more than 55 %) have been exhibited by the film. For strong absorption in shorter wavelength, electron in valance band absorbs some

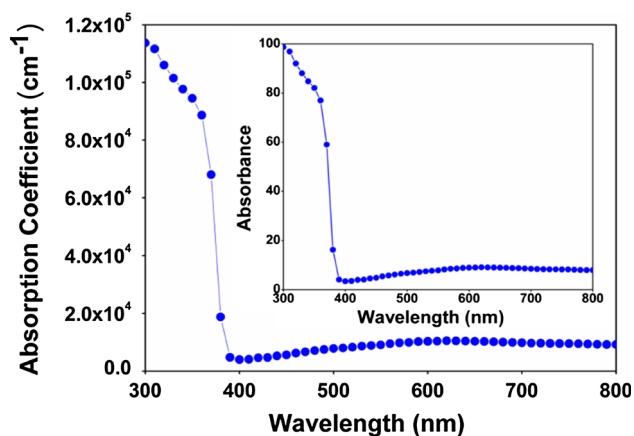


**Fig. 5** Variation of absorption coefficient of ZnO thin film with wavelength, (*inset*) plot of absorbance versus wavelength of ZnO nanoparticles

photon energy and transit into conduction band by creating some hole in valence band i.e. formation of exciton. The excitonic peak is a sign of high optical quality of ZnO and excitonic absorption peaks shows that ZnO thin films have good optical properties. It is clear that ZnO behaves as opaque material for shorter wavelengths and behaves as transparent material for longer wavelengths. The optical bandgap of the thin film is derived from the relation between incident photon energy ( $h\nu$ ) and absorption coefficient ( $\alpha$ ) as given by Eq. (8) [2]:

$$(\alpha h\nu)^2 = A(h\nu - E_g) \tag{8}$$

where,  $h\nu$  is the photon energy, A is constant and  $E_g$  is the optical bandgap of the thin film.

The energy bandgap of thin film can be estimated from the extrapolation of the linear portion of  $(\alpha h\nu)^2$  versus  $h\nu$  plot as shown in Fig. 6. The value of energy bandgap was obtained as 3.24 eV for ZnO thin film. The optical constants such as extinction coefficient ( $k$ ) and refractive index ( $n$ ), calculated for the wavelength range of 300–800 nm are shown in Fig. 7 as a function of wavelength. The extinction coefficient and absorption coefficient are interrelated as [2]:

$$k = \frac{\alpha \lambda}{4\pi} \tag{9}$$

The refractive index ( $n$ ) is related to reflectance, transmittance and extinction coefficient [2]

$$n = \sqrt{\frac{4R}{(1-R)^2} - k^2} + \frac{(1+R)}{(1-R)} \tag{10}$$

where, R is reflection coefficient of ZnO thin film. From Fig. 7 (*inset*) it can be observed that the refractive index initially increases with increase in wavelength and then attains a maximum value around 360 nm after which it

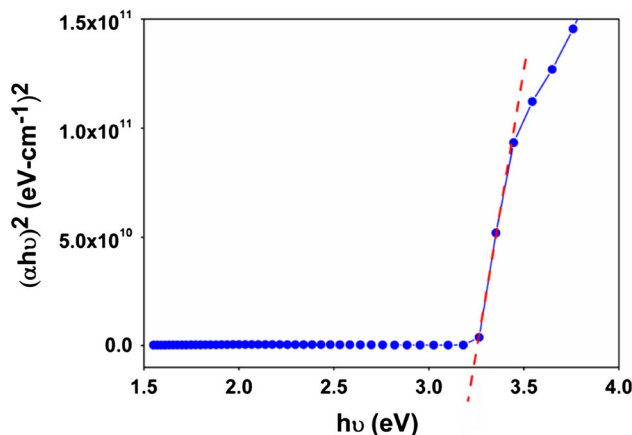


**Fig. 6**  $(\alpha h\nu)^2$  versus  $h\nu$  plot for evaluation of optical bandgap of ZnO nanoparticle thin film

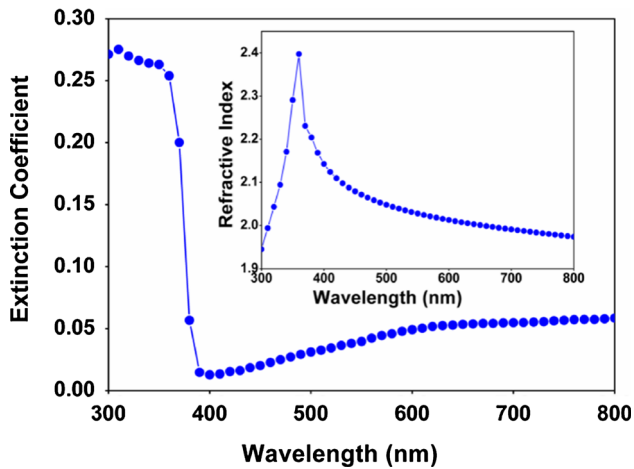


**Fig. 7** Plot of extinction coefficient versus wavelength, (*inset*) plot of refractive index versus wavelength of ZnO nanoparticle thin film

starts decreasing with further increasing wavelength. The highest value of refractive index is approximately 2.397 near the inter band transition. The dielectric constant of thin film can be represented as follows [1]

$$\varepsilon(\lambda) = \varepsilon_{real}(\lambda) + \varepsilon_{img.}(\lambda) \quad (11)$$

The real and imaginary part of dielectric constant can be written as [1]:

$$\varepsilon_{real}(\lambda) = n^2 - k^2 \quad (12)$$

$$\varepsilon_{img.}(\lambda) = nk \quad (13)$$

The variations of the real and imaginary part of dielectric constant with respect to wavelength are shown in Fig. 8. Asharply strong peak value near the bandgap wavelength as observed in the figure indicates that that there is a strong interaction between electrons and holes at

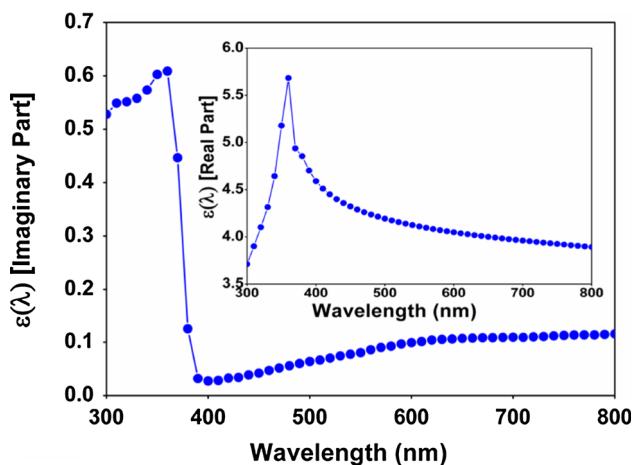


**Fig. 8** Plot of real part of dielectric constant versus wavelength; (*inset*) Plot of imaginary part of dielectric constant versus wavelength of ZnO nanoparticle thin film

this particular wavelength. The volume energy loss (VELF) and the surface energy loss (SELF) functions have been studied to evaluate the rate of energy loss for moving electrons passing through a material [17]. VELF and SELF are related to the real and imaginary parts of the dielectric constant as [17]:

$$\text{Volume energy loss (VELF)} = \frac{\varepsilon_{img.}}{(\varepsilon_{real}^2 + \varepsilon_{img.}^2)} \quad (14)$$

$$\text{Surface energy loss (SELF)} = \frac{\varepsilon_{img.}}{((\varepsilon_{real} + 1)^2 + \varepsilon_{img.}^2)} \quad (15)$$

The variations of VELF and SELF with the photon energy  $h\nu$  are shown in Fig. 9. It is also clear that there is no significant difference between SELF and VELF, particularly at higher photon energies (up to 3.25 eV) but the VELF increases more than SELF at photon energy after 3.5 eV.

In order to investigate the emission characteristics of ZnO nanoparticles, the sol form the ZnO, prior to deposition on Si substrate were examined at room temperature by photoluminescence (PL) spectroscopy. The spectra as shown in Fig. 10 contain a wide visible emission band. It can be seen that the UV emission peak associated to near band edge emission of ZnO nanoparticles is located at 383 nm followed by a very strong violet emission located at 412 nm. This type of co-emission exhibited by double peaks corresponding to the UV emission at 383 nm and the violet emission at 412 nm are rarely reported in ZnO-based thin film material. UV emission is generally attributed to the recombination of free excitons of ZnO [2]. The violet emission mechanism is not very clear but yet some researchers had proposed some emitting models for spectra and the mechanism of emission is not clearly understood [2].

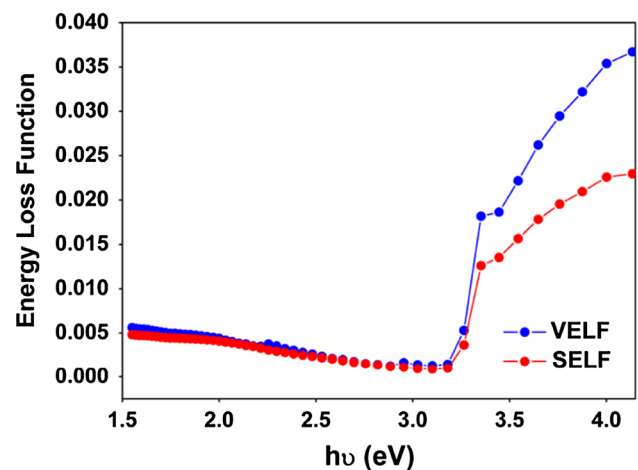


**Fig. 9** Energy loss function of ZnO nanoparticle thin film

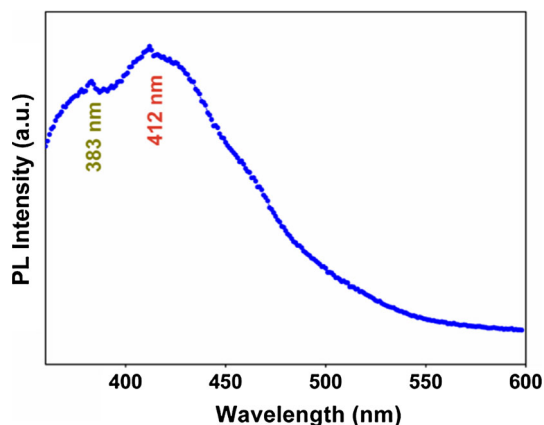


Fig. 10 PL spectra of sol-gel derived ZnO of ZnO nanoparticles

### 3.4 Estimation of electrical and photodetection performance

After a detailed investigation of structural and optical parameters of as-deposited ZnO nanoparticle thin film, the electrical and UV photodetection performance of a ZnO nanoparticle/Si heterojunction diode was studied. Figure 11 shows the current–voltage characteristics of the proposed device under dark and UV light. It can be seen that the device exhibits a typical heterojunction diode characteristics with rectification ratio of 151 and turn on voltage of 0.61 V under dark condition. The barrier height ( $\phi_{bh}$ ) and ideality factor ( $\eta$ ) of the device at room temperature are calculated using the following relations [18]

$$\eta = \frac{q}{kT} \frac{\partial V}{\partial \ln(I/I_0)} \tag{16}$$

$$I_0 = AA^*T^2 \exp(-q\phi_{bh}/kT) \tag{17}$$

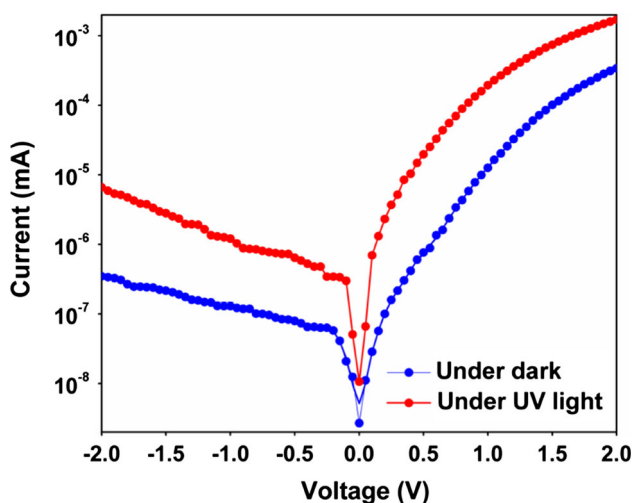


Fig. 11 Current-voltage characteristics of ZnO nanoparticles/Si heterojunction diode

where  $q$  is electronic charge,  $k$  is Boltzmann’s constant and  $T$  is absolute temperature,  $A$  and  $A^*$  are the area and Richardson constant respectively.  $I_0$ , denoted as reverse saturation current or dark current of the diode is directly calculated from  $I$ – $V$  characteristics as 16 nA. Ideality factor ( $\eta$ ) and effective barrier height ( $\phi_{bh}$ ) of the diode are estimated to be 3.13 and 0.73 eV respectively. The values of the electrical parameters suggest that the proposed device can be used as a heterojunction rectifying contact. It may be pointed out here that the ideality factor of the device is higher than 1. It is well understood [18, 19] that high ideality factor ( $\eta > 1$ ) in Schottky contact can be attributed to the several facts including interface states at a thin oxide between the metal and the semiconductor, tunneling currents in highly doped semiconductors or the image force lowering of the Schottky barrier in the electric field at the interface and/or generation/recombination currents within the space-charge region. These four models describe the behavior of Schottky contacts under extreme conditions assuming a spatially homogeneous, more or less atomically flat interface between the metal and semiconductor.

In the case of ZnO thin film based devices the theory of Schottky contact (Metal–semiconductor) is widely used for understanding the mechanism of operation of many thin film devices. However, rigorous models of other semiconductor devices like heterojunctions, MIS, MISIM etc. are not available. Therefore, in typical cases, where the experimental current–voltage characteristics follow the approximately similar behavior as that of Schottky contacts, it is customary to model the device using thermionic emission theory which is dedicated to Schottky contact junctions [20, 21].

On the basis of study involving the temperature dependent characteristics of Si/ZnO interface using thermionic emission theory combined with Richardson model for barrier inhomogeneities, it is claimed by various research groups [22, 23] that barrier inhomogeneities (defects in interface grain boundary formation like dislocation and stacking faults) are certainly present at the interface of Si substrate and as-grown epitaxial ZnO thin film due to large lattice mismatch and thermal coefficient mismatch between Si and ZnO. Greuter and Blatter [24] have also reported that the formation of grain boundaries at the Si/ZnO (compound semiconductor) interface can alter the electrical properties of the Si/ZnO devices. Although, some surface/interface treatment like post-annealing or doping with inert gas (nitrogen, argon) can reduce these inhomogeneities to some extent but it is not possible to remove the inhomogeneity completely. In our present work the epitaxial ZnO nanoparticle film on Si substrate has been obtained by sol-gel spin coating technique followed by annealing at high temperature to promote single crystalline ZnO film growth so as to obtain a near homogeneous Si/ZnO interface. Our

characterization however, revealed that the grown film is actually a polycrystalline ZnO one with a strong urge to grow along c-axis. Therefore, inhomogeneities (though very less) at the Si/ZnO interface cannot be completely ruled out. This in turn affects the electrical transport characteristics of the Si/ZnO heterojunction. This inhomogeneity at the interface is thus responsible for a large value of ideality factor for the device under study.

The ultraviolet photodetection properties of the proposed device are investigated under UV light at 365 nm. Under UV illumination, electron–hole pairs (EHPs) are generated at the interface of ZnO/Si heterojunction and as well as at the surface of ZnO film. When the bias voltage is applied at the ohmic contact, the EHPs are extracted in the external circuit. It may be noted that due to UV light exposure, electron–hole pairs are generated in the depletion region. These photogenerated carriers play the key role in determining the photoresponse of Si/ZnO heterojunction diode under reverse bias. In view of a high barrier height under reverse bias, EHPs generated away from junction cannot cross the junction and as a result they are not able to contribute to the photocurrent in external circuit. However, under forward bias condition the barrier height is lowered by 0.7 eV, due to which the EHPs generated in the ZnO layer contribute to the photocurrent in external circuit [19–21]. The optical parameters including responsivity ( $R$ ) and external photodetection efficiency ( $\eta_{ext}$ ) are calculated using the following expressions [13]:

$$R = I_{ph}/P_{opt} \quad (18)$$

$$\eta_{ext} = 1240 \frac{R}{\lambda} \quad (19)$$

where,  $P_{opt}$  is the incident optical power and  $I_{ph}$  is the output photocurrent, and  $\lambda$  is the wavelength of the UV light. Responsivity and external quantum efficiency of the proposed device are estimated from  $I$ - $V$  characteristics in the illuminated condition as 0.07 A/W and 25 % respectively at 2 V reverse voltage (Fig. 11). The same parameters are also calculated at 2 V forward voltage because it has been observed from the Fig. 11 that the device exhibits good photoresponse both at reverse as well as forward bias voltage. At 2 V forward bias voltage, device has exhibited a UV photoresponsivity of 17.1 A/W.

## 4 Conclusion

The structural, optical and electrical characteristics of the ZnO nanoparticle/p-Si heterojunction photodetector are experimentally measured. The sol–gel synthesized ZnO nanoparticles were characterized completely in respect of surface

morphological and optical properties. It has been observed that the ZnO nanoparticle thin film synthesized by this technique exhibits a good crystalline nature with minimum surface roughness. The optical parameters such as reflectance, transmittance, absorbance, refractive index, real & imaginary part of dielectric constant, energy loss function and photoluminescence spectra demonstrate excellent behavior of the film. The results confirm that a high quality ZnO thin film derived by sol–gel spin coating technique can potentially be used in a variety of optoelectronic devices. The high value of photo-sensitivity of the proposed Si/ZnO device suggests its possible application in highly sensitive UV detectors.

## References

1. S. Sharma, S. Vyas, C. Periasamy, P. Chakrabarti, Superlattices Microstruct. **75**, 378 (2014)
2. L. Xu, G. Zheng, H. Wua, J. Wang, F. Gu, J. Su, F. Xian, Z. Liu, Opt. Mater. **35**, 1582 (2013)
3. A.-S. Gadallah, M.M. El-Nahass, Adv. Cond. Matter Phys. **2013**, 234546 (2013)
4. M. Sahal, B. Hartiti, A. Ridah, M. Mollar, B. Mari, Microelectron. J. **39**, 1425 (2008)
5. P.-Y. Lee, S.-P. Chang, J.-F. Chang, E.-H. Hsu, S.-J. Chang, Int. J. Electrochem. Sci. **8**, 6425 (2013)
6. M. Ohyama, H. Kozuka, T. Yoko, Thin Solid Films **306**, 78 (1997)
7. A. Rajan, H.K. Yadav, V. Gupta, M. Tomar, J. Mater. Sci. **48**, 7994 (2013)
8. B. Gupta, A. Jain, R.M. Mehray, J. Mater. Sci. Technol. **26**, 223 (2010)
9. A. Tataroğlu, H. Aydın, A.A. Al-Ghamdi, F. El-Tantawy, W.A. Farooq, F. Yakuphanoglu, J. Electroceram. **32**, 369 (2014)
10. K.J. Chen, F.Y. Hung, S.J. Chang, S.J. Young, Mater. Trans. **50**, 922 (2009)
11. F. Yakuphanoglu, Y. Caglar, M. Caglar, S. Ilcan, Mater. Sci. Semicon. Process **13**, 137 (2010)
12. K.L. Foo, M. Kashif, U. Hashima, M.E. Ali, Optik **124**, 5373 (2013)
13. G.M. Ali, P. Chakrabarti, I.E.E.E. Photon, J. **2**, 784 (2010)
14. K. Huang, Z. Tang, L. Zhang, J. Yu, J. Lv, X. Liu, F. Liu, Appl. Surf. Sci. **258**, 3710 (2012)
15. J. Sengupta, A. Ahmed, R. Labar, Mater. Lett. **109**, 265 (2013)
16. S. Singh, P. Chakrabarti, Superlattices Microstruct. **64**, 283 (2013)
17. H.A. Mohamed, Optoelectron. Adv. Mat. **6**, 389 (2012)
18. F. Yakuphanoglu, Phys. B **388**, 226 (2007)
19. J.H. Werner, H.H. Guttler, J. Appl. Phys. **69**, 1522–1533 (1991)
20. O. Pakma, N. Serin, T. Serin, Ş. Altındal, J. Appl. Phys. **104**, 014501 (2008)
21. F. Yakuphanoglu, Phys. B **388**, 226–229 (2007)
22. S. Majumdar, P. Banerji, J. Appl. Phys. **105**, 043704 (2009)
23. D. Somvanshi, S. Jit, IEEE Trans. Nanotechnol. **13**(1), 62–69 (2014)
24. F. Greutert, G. Blatter, Semicond. Sci. Technol. **5**, 111–137 (1990)